PPPL-2175

UC20-A,F

I-18948

PPPL-2175

DR-0732-23

191
1-17-85 QS ②

PARTICLE FUELING AND IMPURITY CONTROL IN PDX

By

R.J. Fonck et al.

DECEMBER 1984

PLASMA PHYSICS LABORATORY

PRINCETON UNIVERSITY
PRINCETON, NEW JERSEY

PREPARED FOR THE U.S. DEPARTMENT OF ENERGY,
UNDER CONTRACT DE-AC02-76-CHO-3073.

NOTICE

Printed in the United States of America

Available from:

National Technical Information Service
U.S. Department of Commerce
5285 Port Royal Road
Springfield, Virginia 22161

Price Printed Copy $ * ; Microfiche $4.50

*Pages	NTIS Selling Price
1-25	$7.00
25-50	$8.50
51-75	$10.00
76-100	$11.50
101-125	$13.00
126-150	$14.50
151-175	$16.00
176-200	$17.50
201-225	$19.00
226-250	$20.50
251-275	$22.00
276-300	$23.50
301-325	$25.00
326-350	$26.50
351-375	$28.00
376-400	$29.50
401-425	$31.00
426-450	$32.50
451-475	$34.00
476-500	$35.50
500-525	$37.00
526-550	$38.50
551-575	$40.00
567-600	$41.50

For documents over 600 pages, add $1.50 for each additional 25-page increment.

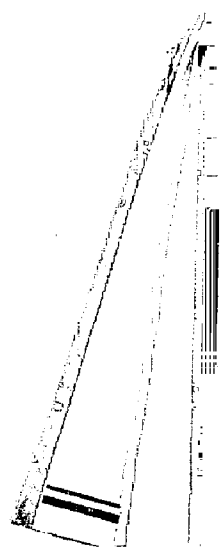

PPPL--2175

DE85 005350

PARTICLE FUELING AND IMPURITY CONTROL IN PDX[†]

R. J. Fonck, M. Bell, K. Bol, R. Budny, P. Couture[*], D. Darrow, H. Dylla, R. Goldston, B. Grek, R. Hawryluk, K. Ida, K. Jaehnig, D. Johnson, R. Kaita, S. Kaye, H. Kugel, B. LeBlanc, D. Mansfield, T. McBride, K. McGuire, S. Milora[**], D. Mueller, M. Okabayashi, D. Owens, D. Post, M. Reusch, G. Schmidt, S. Sesnic, H. Takahashi, F. Tenney, and M. Ulrickson

Plasma Physics Laboratory, Princeton University
Princeton, NJ 08544 (USA)

ABSTRACT

Fueling requirements and impurity levels in neutral-beam-heated discharges in the PDX tokamak have been compared for plasmas formed with conventional graphite rail limiters, a particle scoop limiter, and an open or closed poloidal divertor. Gas flows necessary to obtain a given density are highest for diverted discharges and lowest for the scoop limiter. Hydrogen pellet injection provides an efficient alternate fueling technique, and a multiple pellet injector has produced high density discharges for an absorbed neutral beam power of up to 600 kW, above which higher speeds or more massive pellets are required for penetration to the plasma core. Power balance studies indicate that 30-40% of the total input power is radiated while ~ 15% is absorbed by the limiting surface, except in the open divertor case, where 60% flows to the neutralizer plate. In all operating configurations, Z_{eff} usually rises at the onset of neutral beam injection. Both open divertor plasmas and those formed on a well conditioned water-cooled limiter have $Z_{eff} \lesssim 2$ at the end of neutral injection. A definitive comparison of divertors and limiters for impurity control purposes requires longer beam pulses or higher power levels than available on present machines.

[†]Presented at the 6th International Conference on Plasma Surface Interactions in Controlled Fusion Devices, Nagoya, Japan, 14-18 May 1984.
[*]IREQ Institut de recherche d'Hydro-Quebec, Canada.
[**]Oak Ridge National Laboratory, Oak Ridge, TN, USA.

1. Introduction

As experience with large auxiliary-heated tokamak devices has grown, the importance of impurity control has become ever more evident. High power neutral beam injection experiments in several devices have allowed the study of impurity production and control under power loading levels of several kW/cm^2. Advanced limiter concepts such as toroidal limiters [1,2] and particle scoop limiters [3,4] are presently under study while large tokamaks with magnetic divertors have been operating for several years [5-7]. Tests of these concepts for impurity control are particularly important for the design of future long pulse devices with high power loading. The importance of particle control in tokamaks has also increased dramatically in the past few years. The localization of the plasma fueling source near the divertor region has been identified as a crucial factor in the attainment of improved energy confinement in neutral-beam-heated divertor discharges [8-10], while the use of pellet fueling has led to the attainment of breakeven values of $n\tau$ in the Alcator-C device [11].

Earlier, we reported a preliminary comparison of several impurity control devices in the Poloidal Divertor Experiment (PDX) tokamak [5]. That work emphasized the need to explore more fully several impurity control techniques in the presence of high power auxiliary heating. The PDX device is a large tokamak (R_p = 145 cm, a = 40 cm) with up to 6 MW of neutral beam heating power available for 300 ms, and it has been capable of producing plasmas with either standard rail limiters, a toroidal bumper limiter, both open and closed poloidal divertors, and a particle scoop limiter. Plasma fueling is achieved by either gas puffing or hydrogen pellet fueling. The main experiments in PDX consisted of the study of heating efficiency with near-perpendicular injection (each of four beam lines on PDX have a tangency

radius of 35 cm), the study of high-β, low q(a) discharges, and exploring regimes of improved confinement with diverted and scoop limiter discharges. During these studies, we have expanded our data base on the performance of various particle and impurity control techniques during high power neutral injection. In this paper, we review information obtained in the past two years to gain more insight into a direct comparison of these techniques for particle and impurity control, and to put our earlier results in better perspective.

Several modifications were made to the PDX device in late 1982 to extend the machine capabilities and allow new modes of operation [8]. The divertor hardware was modified to close off the open conductance paths between the divertor chambers and the main plasma chamber, so that recombined neutral particles in the divertor region could enter the main chamber only by passing through the plasma in the throat region. This configuration is referred to as the "closed" divertor mode, as distinguished from the earlier "open" mode of operation. The outer divertor coils were deactivated to ease the plasma startup. The titanium divertor neutralizer plates and liners in the main chamber were replaced with ones made of stainless steel. In addition, the practice of Ti gettering in the upper divertor region was discontinued so that the upper chamber was unpumped. With these changes, single-lobe diverted plasmas of up to 500 kA with R = 140 cm and a ≈ 38 cm could be obtained routinely by displacing the plasma column a few cm upward, and our earlier problems with titanium bursting in divertor plasmas were alleviated.

In addition to the divertor modifications, a particle scoop limiter was installed on the outer vacuum vessel wall. This limiter is described in detail elsewhere [3], but we note here that it consists of a large (29 cm x 33 cm) front graphite surface with a 2-cm wide pumping channel approximately 2 cm

behind the front face. The plasma hits vanadium-coated copper neutralizer plates and the recombined neutrals are collected in an unpumped 50-ℓ closed volume behind the limiter surface. The limiter was at a major radius of 193 cm, resulting in 40-cm radius plasmas with R_p = 153 cm.

We concentrate here on discussions of the rail limiter, scoop limiter, and inside Dee divertor discharges with neutral injection. Four-null divertor discharges and toroidal bumper limiter discharges were discussed in our earlier paper [5].

The major diagnostics employed for these studies include Thomson scattering systems for both the central plasma and edge plasma measurements, while impurities are monitored with absolutely calibrated VUV spectrometers, an X-ray pulse height analysis system, bolometer arrays, and visible bremsstrahlung measurements. Power deposition and edge plasma power flows are inferred from infrared TV observations, thermocouple arrays, and a variety of plasma probes.

2. Fueling and Particle Control

2.1 Gas Puffing

The fueling of ohmically heated PDX discharges by puffing cold gas at the plasma periphery has been described in detail previously [12,13]. In general, the diverted discharges, either open or closed, required the largest gas flow to sustain a given plasma density while the limiter discharges required the least (approximately four times less than the divertor case), with the toroidal bumper limiter falling roughly midway between these two extremes. The change in neutral gas behavior, which was most evident after closing the divertor, was the buildup of a neutral gas pressure difference between the divertor and main chamber regions. While the compression ratio, P_{DIV}/P_{MAIN}, was very close to unity for all cases with the open divertor

configuration, it routinely reached values of 10 to 30 in the closed configuration. Neutral gas pressures approaching 10^{-3} Torr were achieved in the divertor region for line average densities of ~ 5 x 10^{13} cm^{-3} (fig. 1). Both the neutral pressure and the scrape-off plasma density showed a nonlinear increase with the average main plasma density, indicating that a high recycling divertor regime was achieved. The dependence of neutral pressure, H_α emissions, and divertor plasma density on $\bar{n}_e$ was modeled with the DEGAS neutral transport code to indicate that the electron temperature in the divertor region was a rapidly falling function of $\bar{n}_e$, with values below 10 eV for $\bar{n}_e \gtrsim 3 \times 10^{13}$ cm^{-3} [13,14].

The situation with neutral beam injection (NBI) is considerably more complex since the confinement behavior of the plasma itself is a sensitive function of the operating conditions [3,9]. It is instructive, however, to compare the gas flow rates required to achieve or sustain a given plasma density during at least 200 ms of NBI for each of our operating modes. In table 1 we list the gas flow rate required to obtain the listed $n_e\ell$ for each of five operating conditions of interest. The open divertor results were obtained with the upper dome ungettered, similar to the closed divertor operating conditions. Neutral gas pressures were measured with magnetically shielded ionization gauges located near the limiter (rail or scoop) on the plasma midplane and in the upper divertor dome. The ionization gauge near the limiters was located on the outside wall of the vacuum vessel, directly below the scoop limiter. Since the top rail limiter was used in the rail limiter studies, this gauge was located considerably closer to the scoop surface than to the surface of the graphite rail.

The rail-limited discharge shows a relatively high pressure near the limiter while it is quite low far away from the limiter. The pressure

near the scoop limiter was less than, but comparable to, the values obtained with the rail limiters. However, the scoop requires a very low gas flow compared to the rail limiter, suggesting efficient recycling on the face of the scoop or through the volume of gas trapped in the scoop plenum. The pressure of this gas in the plenum is on the order of 10^{-2} Torr.

The neutral gas distribution in diverted discharges with NBI is compared in table 1 for three cases of interest. The open divertor data show only a slight amount of compression between the unpumped divertor region and main chamber. The operation mode designated H-mode is an example of the improved confinement regime obtained with diverted discharges with NBI [8,9]. This regime, originally observed on the ASDEX device [15], is characterized by a spontaneous improvement in the particle confinement time during NBI and hence high values of $\bar{n}_e$ are obtained with moderate gas feeds. The second regime of operation in the closed divertor geometry is identified by a forced density rise (FDR) wherein the gas feed is increased to force the density to rise up to or above values it would achieve in a good high confinement H-mode shot. These FDR discharges are characterized by lower confinement times typical of open divertor and limiter discharges. A necessary characteristic for the achievement of high confinement in PDX has been a large compression ratio and low main chamber neutral gas pressure. As seen in table 1, this feature is lost in the FDR case where neutral gas is forced back to the main chamber through the divertor scrape-off plasma or through residual open conductances in the divertor/main chamber interface hardware. Calculations of the neutral particle transport in diverted PDX discharges with NBI have been reported by Heifetz et al. [14].

Finally, the toroidal and poloidal distributions of H_α or D_α emissions give insight into the particle source locations. The toroidal

distribution of H_α/D_α emissions shows a large peak near the limiter in rail and scoop limited discharges, while a large peak at the location of the midplane gas puffing valve was observed for the open divertor case [12,16]. In the closed divertor case with a divertor gas feed, the toroidal distribution is essentially flat, but the poloidal distribution shows a strong localization of the particle source in the region of the divertor throat [9,17,18].

2.2 Pellet Injection

An alternative fueling mechanism is the injection of solid hydrogen pellets at high speed (600-900 m/s) into the plasma. Early single pellet injection experiments into diverted PDX discharges with only ohmic heating have already been described elsewhere [19]; here we give an overview of results obtained with multiple pellet injection into diverted discharges with and without NBI. The injector used was capable of injecting three hydrogen pellets ($\sim 1.5 \times 10^{20}$ atoms/pellet) with arbitrary differences in the injection time for each pellet.

Pellet injection has produced ohmic discharges with much higher density than those available with gas puffing. For ~ 300 kA ohmic discharges, the large pellets are able to penetrate beyond the plasma axis, resulting in a substantial peaking of the particle deposition on the central flux surfaces. For example, ohmically heated plasmas with $n_e(o) = 3 \times 10^{14}$ cm^{-3} have been produced by injection of three closely spaced pellets ($\Delta t \lesssim 5$ ms). The Murakami parameter, $\bar{n}_e R/B_T \sim 9.5$, is substantially higher than that obtained with gas puffing. The plasma absorbed this extra fuel without disruption, and the global interaction with the fuel is observed to be approximately adiabatic. Immediately following injection, the electron temperature is greatly reduced, but recovers rapidly. Density and temperature profiles

obtained via Thomson scattering immediately before and after pellet injection are shown in fig. 2. After this abrupt density rise, sawtooth oscillations are suppressed while the central density decays with a characteristic decay time of 100-150 ms. The density profiles remain strongly peaked during this decay.

In discharges with NBI, the pellet penetration is substantially reduced since the ablation rate is increased due to both the higher electron temperatures in beam-heated plasmas and the additional ablation due to fast beam ions [20]. For a given injected beam power, the beam ion contribution may be enhanced even more with perpendicular injection, as in PDX, since a large fraction of the ions are trapped in orbits on the outboard side of the plasma, particularly at large minor radii. It appears that a significant perturbation in the plasma density profile occurs only when the pellets penetrate the plasma to near the $q = 1$ surface. For the existing pellet injector with a pellet speed of ~ 800 m/s, a single pellet penetrates to only $r/a \sim 0.5$ for $P_{abs} = 2$ MW, where P_{abs} is the absorbed neutral beam power. The use of several pellets spaced closely in time ($\Delta t \simeq 1$ to 2 ms), however, does improve penetration and results in particle deposition inside the $q = 1$ surface for low beam power. For example, fig. 3 shows the change in the central chord visible continuum radiation (roughly proportional to $\bar{n}_e^2$) for beam-heated discharges with pellet injection. The incremental change in the signal at the time of pellet injection gives a measure of the overall density increase due to the pellets. As the beam power increases, the penetration decreases, but it can be improved somewhat by stacking all three large pellets closely in time, effectively simulating injection of a pellet with larger mass.

Using two closely spaced pellets, discharges with peak $n_e(o) \sim 1 \times$

10^{14} cm^{-3} were produced with P_{abs} = 0.6 MW for detailed study. The central density remains high and the density profile remains peaked as the T_e and T_i profiles recover after pellet injection. During this period, an increase in the global confinement time from 20 to 30 ms occurs, while MHD fluctuations change from sawtooth oscillations before pellet injection to m = 1 oscillations afterward.

Although a detailed comparison has not been made, pellet fueling with penetration to the q ~ 1 surface is considerably more efficient than gas puffing. The fraction of injected atoms which are converted to plasma ions is ~ 1 for the ohmic case and ~ 0.5 for the 0.6 MW beam-heated cases. The corresponding fueling efficiency for gas puffing is ~ 0.1 or less for high density ohmic plasmas [12], and is estimated to be comparable to or lower than this value for the beam-heated discharges.

3. Energy Deposition and Power Balance

3.1 Graphite Rail Limiter

Earlier, we reported on the properties of undiverted plasmas formed on standard carbon rail limiters at a single toroidal location [5]. The uncooled limiters were often disruptive during high power NBI($P_{INJ} \gtrsim 6$ MW) for beam pulse lengths of $\gtrsim$ 150 ms. In general, however, these discharges with $P_{INJ} < 6$ MW had negligible metallic impurity content, and radiated power profiles obtained with a bolometer array were hollow, with total radiated powers accounting for ~ 30% of the input power. It was noted at the time that spectroscopic estimates of radiated power were only ~ 1/2 the values obtained with the bolometer measurements, and the discrepancy was ascribed to the bolometer sensitivity to fast charge exchange neutrals arising from the anisotropic beam ion velocity distribution. This suggestion has since been studied in more detail [21], and substantively confirmed by comparing the

bolometer signal from different angles of view with respect to the toroidal field. In addition, the contribution of the fast neutrals themselves to the bolometric measurements was estimated by studying the exposure of poly-methyl-methacrylate (PMMA) to the energy flux at the vessel wall. All these methods indicate that up to 50% of the flux to the standard bolometer array on PDX can be accounted for by beam charge exchange. A measurement of the toroidal asymmetry in bolometric power loss measurements was made by placing a bolometer near the limiter location. The ratio of the power loss near the limiter to that 126° away toroidally (i.e., the standard bolometer location) was ~ 1.8 for ohmic discharges while it rose to ~ 3.5 for discharges with strong NBI. If we take the radiated power toroidal distribution to be similar to that measured for H_α emissions [16], we estimate that the total power loss is at least 1.4 times that given by the local bolometer array measurements.

At the end of 1981 the rail limiters were modified to allow water cooling between shots to keep the bulk limiter temperature below 100°C before the next discharge [22]. A single graphite rail limiter of this type was subsequently used for low q(a), high $\langle\beta_T\rangle$ experiments from February to July 1982. In initial operation, a disruption would usually occur shortly after the start of neutral beam injection due to a large influx of impurities, principally carbon. However, operation over a period of several months resulted in sufficient conditioning of the limiter surface that 6 MW of NBI could be handled for 250 ms without disruption. Detailed surface analysis indicates that a thin TiC coating had formed on the limiter surface by the end of this operation period [23].

Similar to the results obtained with the uncooled limiters, power fluxes of ~ 3 kW/cm^2 and surface temperatures of ~ 1400°C were typical with high beam powers ($P_{INJ} \gtrsim 3$ MW). In general, the energy deposition on the

limiter varied from 15 to 30% of the input energy (E_{IN}) and tended to saturate at high E_{IN} [22]. Bolometric estimates of volume-integrated radiated power losses average ~ 30% of the input power. Some of the remaining 40-50% of the input power, which is still unaccounted for, can be found in the above-mentioned toroidal asymmetry of radiation losses, although a strict accounting requires a detailed measurement of the toroidal and poloidal radiated power distribution.

3.2 Divertor Discharges

The energy balance and power loading of open divertor discharges with NBI was discussed in Ref. 5, and here we concentrate our discussion on results obtained principally with the closed divertor geometry and an open geometry with an ungettered upper dome. The energy balance of these diverted discharges in PDX has been discussed in some detail by Bell et al. [16]. In general, the largest difference between the open and closed divertor cases occurs in the fraction of input energy which is deposited on the divertor neutralizer plates. In the open divertor case with NBI, this energy to the plates was typically 50-60% of the input energy while it ranged from 11 - 17% for the closed divertor case. Almost all of this energy was deposited on the outer neutralizer in both cases. The average energy deposition on the neutralizer plate was measured by a thermocouple array and by probe measurements of the divertor plasma [24]. A comparison of the thermocouple array results and the integrated energy flux from probe data projected along magnetic fields lines to the outer neutralizer plate is shown in fig. 4 for a good H-mode discharge with P_{INJ} = 2.3 MW. Reasonable agreement between the two measurements is obtained, and the peak power fluxes are ~ 0.2 kW/cm^2. Also, the power deposition profile width is quite narrow, ~ 2 cm, in contrast to the high neutral pressure data obtained with the open divertor at high

plasma densities [5].

Bolometric measurements indicate that 30-40% of the input power is radiated in the main chamber while $\lesssim$ 5% is radiated in the divertor chamber. Some of the remaining power can be accounted for by a large asymmetry in the bolometer profiles observed near the divertor throat region in the main chamber. Up to ~ 15% of the input power was estimated to be radiated from this region for ohmically heated plasmas, and this asymmetry broadens considerably during NBI. The quoted values for radiated power ignore this asymmetry by inverting the bolometer data from the lower half of the plasma. The broad divertor throat radiation can cause the inverted profiles from the lower half to appear more peaked in the center than they really are, but spectroscopic estimates of impurity radiation from the plasma center indicate that the central radiation density is at most 100-200 mW/cm^3.

Thus while energy accountability was reasonably good for the open divertor case, it is considerably poorer for the closed divertor case. Efforts are underway to determine if the enhanced radiation near the divertor throat is sufficiently intense to account for the missing input energy.

3.3 Particle Scoop Limiter

The power loading on the front face of the unpumped scoop limiter was studied by using an infrared camera to scan the midplane front face temperature. The surface temperature and power loading was very similar to that of the carbon rail limiter. Peak surface temperatures of ~ 1400°C and power fluxes up to 3 kW/cm^2 were observed at $P_{abs} \gtrsim 3$ MW. With its larger front face area, this limiter absorbs 25-50% of the total input power, which is higher than the typical values for a rail limiter. The wide variation in this fraction is due to variations in operating conditions such as plasma density, current, position, etc. Toroidally asymmetric thermal loads were

observed on the scoop limiter. The asymmetry was usually skewed toward the beam ion drift direction and tended to increase with P_{INJ}. Ion orbit calculations indicate that 20-40% of the total thermal load is due to bad ion orbit losses, consistent with the magnitude and direction of the observed asymmetries. Calorimeter probe measurements of the power flow in the plasma scrapeoff indicate that a total of only 60 kW, or 3% of P_{Total} ($\sim$ 2 MW), flows into the scoop channel [25]. Finally, bolometer estimates of radiated power losses account for 20-40% of the total input power. Efforts are underway to reduce the uncertainties in both the absorbed energy fraction and the radiated power estimates to see if there still exists a substantial fraction of the input power unaccounted for.

4. Impurity Levels During Neutral Injection

We should note immediately that the impurity levels in PDX discharges are seldom so great as to perturb the plasma significantly. With the exception of some of the closed divertor cases and cases with counter-injection, radiated power losses in the plasma core are only a small fraction ($\lesssim$ 10%) of the input power and do not significantly affect the overall power balance there. However, it is instructive to examine the plasma purity in order to compare the various options for limiting surfaces. Also, it will be seen that the average values of Z_{eff} obtained with high power NBI are often above levels desired for reactor plasmas. All the data discussed here are for co-injection cases only.

The average impurity level is conveniently characterized by the average plasma Z_{eff}. Since visible continuum measurements in PDX have indicated that the Z_{eff} radial profile is approximately flat for most cases of interest, we use the line-averaged Z_{eff} derived from the central chord continuum emission as a simple impurity monitor. It was found that Z_{eff} rose with the onset of

NBI in almost all running conditions. Figure 5 gives the time evolution of the average Z_{eff} for several cases of interest. As can be seen, only the water-cooled, well-conditioned graphite limiter case actually shows a decrease at the onset of NBI, and this decrease is due mainly to the rapidly rising density.

The cleanliness of rail-limited and open divertor plasmas was discussed earlier in Ref. 5. In general, low-Z impurities were the dominant impurities while titanium was the most abundant metallic impurity, in concentrations of $n_{Ti}(o)/n_e(o) \lesssim 10^{-3}$, or even less under conditions of heavy gas puffing. With such levels, central radiation levels were less than ~ 50 mW/cm^3, and hollow radiation profiles resulted. The later cases of the conditioned rail limiter and the ungettered open divertor were similar, except for occasional bursts of titanium radiation during divertor operation. Edge radiation from low charge states of C relative to characteristic OVI emissions was approximately two times higher for the conditioned limiter case than for the uncooled unconditioned limiter, and titanium radiation was often so low as to be undetectable in these cases. This indicates that in the best cases the cooled rail limiter discharges were almost entirely free of metallic impurities.

The particle scoop limiter appears to behave in some ways like the unconditioned rail limiter, which is not surprising since only seven run days with neutral injection were available for operation with this limiter, and it clearly was not optionally conditioned in that short time. X-ray pulse height analysis measurements indicate iron to be the most abundant metallic impurity in concentrations of (1-4) x 10^{-4} of the electron density, with the balance of Z_{eff} being due to C and O.

The closed divertor case is somewhat extraordinary in that relatively high metallic (principally iron) impurity levels were the norm during NBI. X-ray PHA results show that the iron levels increase rapidly at the onset of

NBI, and the concentration decreases at later times due more to rising plasma density than decreased Fe levels. VUV spectroscopy measurements of good H-mode discharges have given $n_{Fe}(o)/n_e(o) = (3.7 \pm 0.9) \times 10^{-3}$ at early times in the NBI pulse and 1.8×10^{-3} at late times after the density rise which is characteristic of H-mode discharges. Central radiated powers due to iron are ~ 150 mW/cm^3 at early times and ~ 110 mW/cm^3 at late times. Much of the rise in Z_{eff} which occurs at the onset of NBI can often be attributed to increased iron levels. The source of this iron is not definitely known, but most likely arises from plasma interaction with the stainless steel neutralizer plates or liners in the region of the divertor throat. With the exception of a few arc tracks, visual inspection of the liners showed no obvious polishing or damage which would indicate strong plasma-surface interaction.

In our previous report [5], our best data to date indicated that the divertor operation with NBI resulted in cleaner plasmas than either the rail as toroidal bumper limiter operation modes. Since then, however, we have found the cooled graphite limiter to give equivalent results, and the impurity control advantage of the divertor is no longer obvious for PDX discharges.

Continuing such investigations, we have collected values of $\bar{Z}_{eff}$ from visible bremsstrahlung measurements for several operating modes, and these values are plotted in fig. 6 for times at least 200 ms after the onset of NBI. The error bars indicate the standard deviation obtained over several shots during a particular run while the points without error bars reflect values obtained from only one or two shots. While the scatter of data is large, it is noted that relatively clean discharges at high beam powers were obtained with both the open divertor and the conditioned rail limiter, while the closed divertor results were usually poorer due to the large iron concentrations. The exceptionally high datum for the closed divertor at $P_{INJ} = 2.2$ MW came from a series of runs in which the plasma separatrix was shifted

downward a few cm from its usual position. That these results were so dirty indicates that even the divertor neutralizer plates must undergo some conditioning before relatively clean plasmas are obtained. The scoop limiter data are somewhat higher than the best rail limiter data, probably reflecting the relatively short run time available for the scoop.

The present data base is insufficient to unravel any specific dependences of Z_{eff} on discharge parameters such as B_T, I_p, etc. Examination of scalings of Z_{eff} with I_p or B_T indicate that any such dependence is masked by a dependence on varying plasma densities. In order to eliminate the effect of variations in n_e, we plot the quantity $\bar{n}(Z_{eff} - 1)$ as a function of P_{INJ} in fig. 7 for the data shown in fig. 6. Only the very high Z_{eff} closed divertor data were ignored since they were not obtained under standard divertor operating conditions. Neglecting variations in plasma ion dilution due to impurities and in profile effects, $\bar{n}_e(Z_{eff} - 1) \approx \sum_z Z^2 \bar{n}_z$ where $\bar{n}_z$ is the average density of impurity species with ionic charge Z. Thus the plots in fig. 7 give rough estimates of the relative variations of impurity densities as a function of P_{INJ} for each operating mode. Again, the error bars indicate the standard deviation of several shots while points without error bars are due to one or two discharges only. If the impurity densities are constant, this quantity would also be constant. We see that it increases strongly for the rail limiter cases as P_{INJ} increases, indicating increasing impurity densities as P_{INJ} increases. We note, however, that this increase is not observed for low plasma currents ($I_p < 300$ kA) when Z_{eff} values are obtained from Thomson scattering profiles using a Spitzer resistivity model. The lack of such a dependence on P_{INJ} at low I_p may be related to the observation that a lower fraction of the input energy is absorbed by the limiter at low currents than at high currents [22]. The scoop data lie above most of the

rail limiter values except at highest P_{INJ}. This is probably a reflection of the short time spent in operation of the scoop, and its relatively unconditioned state. The open divertor data are quite independent of P_{INJ} except for the low beam power case, while the closed divertor case also indicates a weaker dependence on P_{INJ} than the rail limiters. A cursory look into the difference between the open and closed divertors indicates that it can at least sometimes be ascribed to high iron levels in the closed divertor plasmas. The divertor data as yet show no strong upward trend with P_{INJ} as do the rail and scoop limiters.

Finally, we report an interesting observation of impurity behavior in the presence of pellet injection fueling. Figure 8 presents X-ray PHA results for the impurity levels in a closed divertor discharge with pellet injection and 600 kW of absorbed neutral beam power. At the time of the pellet injection, a large density rise occurs and the X-ray enhancement factor decreases to a value of 1, which is ~ 2 times less than that expected from dilution alone. Z_{eff} drops from 1.8 to 1.0 and recovers slowly, while a drop due to dilution of the plasma with pure hydrogen would result in a value of no less than 1.2. Estimates from visible bremsstrahlung measurements also indicate that Z_{eff} drops to 1, which is significantly lower than that expected from dilution alone. These results suggest that the pellet fueling process is aiding in the expulsion of impurities from the plasma. While these results are preliminary, they may point to an additional benefit of pellet fueling.

5. Summary

We have extended our previous investigations of particle and impurity control to include pellet fueling and discharges formed with a closed high recycling divertor system or an unpumped particle scoop limiter. The gas load required to fuel a scoop limited plasma is significantly lower than a rail limiter, while the closed divertor case can be adequately fueled with

considerably less gas than the old open divertor. Substantial neutral gas pressures can be sustained in either the scoop plenum or closed divertor region with relatively low pressures in the plasma main chamber.

Pellet injection provides an attractive alternative to gas puffing at the plasma edge as a fueling method. Very high density ohmic discharges have been obtained in a moderate toroidal field without disruption. The present injector system is capable of centrally fueling a discharge with modest beam power ($\lesssim$ 600 kW), and the resulting discharges display improved confinement over that of the prepellet plasma. Central fueling with higher beam powers requires larger and/or faster pellets than were available on PDX. There is some evidence that pellet fueling also helps to flush out central impurities from the plasma.

Comparison of impurity levels determined from visible bremsstrahlung measurements and power balance for several modes of operation indicates that while very clean discharges with high neutral injection power can be obtained with both an open divertor and a graphite rail limiter, the limiter data often show an increasing impurity density as P_{INJ} increases when the diluting effect of increasing plasma density is taken into account. This observation raises the question of the ability of limiter discharges to sustain favorable impurity performance under increasing pulse lengths and power loading. The apparent advantage of the divertor over the graphite limiter appears only near the end of our accessible parameter range, and it would be of interest to pursue such comparisons to higher power levels in order to differentiate more clearly between the power handling and impurity generation capabilities of these configurations. The testing of the presumably more favorable power handling abilities of a divertor geometry for high power pulses longer than our 300 ms beam pulse is thus highly desirable.

Acknowledgments

The authors would like to thank the PDX technical crew for assistance in the maintenance and operation of the machine. The support of P. Rutherford and D. Meade throughout the PDX project is greatly appreciated. This work was supported by the United States Department of Energy Contract Number DE-AC02-76-CHO-3073.

TABLE I. GAS FUELING OF NEUTRAL BEAM HEATED DISCHARGES

Configuration	$n_e \ell$ (10^{15} cm^{-2})	Species	P_{INJ} (MW)	Flow Rate Torr-ℓ/sec	P_1(Main) (Torr)	P_2(Div) (Torr)
Rail Limiter	3.4	$D^\circ + H^+$	2.5	56	9.6×10^{-5}	1.3×10^{-5}
Scoop Limiter	3.3	$D^\circ + H^+$	2.3	2.6	7.3×10^{-5}	1.0×10^{-5}
Open Divertor	3.1	$H^\circ + D^+$	2.0	115	9.9×10^{-5}	1.6×10^{-4}
	2.6	$D^\circ + D^+$	2.7	80	4.1×10^{-5}	7.3×10^{-5}
Closed Divertor(H)	2.6	$D^\circ + D^+$	2.2	20	9.3×10^{-5}	1.6×10^{-4}
(FOR)	4.6	$D^\circ + D^+$	2.0	150	3.0×10^{-4}	$> 10^{-3}$

References

[1] M. Ulrickson and H. W. Kugel, Nucl. Tech/Fusion 4 (1983) 141.

[2] H. Vernickel et al., J. Nucl. Mater. 111 & 112 (1982) 317.

[3] R. Budny et al., Princeton Plasma Physics Laboratory Report PPPL-2061 (1983), J. Nucl. Mater. 121 (1984) 285.

[4] P. Mioduszewski, J. Nucl. Mater. 111 & 112 (1982) 253.

[5] R. J. Fonck et al., J. Nucl. Mater. 111 & 112 (1982) 343.

[6] M. A. Mahdavi et al., J. Nucl. Mater. 111 & 112 (1982) 355; and M. Shimada et al., J. Nucl. Mater. 111 & 112 (1982) 361.

[7] M. Keilhacker, Sov. J. Plasma Phys. 9 (1983) 55.

[8] S. M. Kaye et al., J. Nucl. Mater. 121 (1984) 115.

[9] R. J. Fonck et al., in Proceedings of the 4th Int'l. Symposium on Heating in Toroidal Plasmas, Rome, Italy, 21-28 March 1984.

[10] M. Nagami et al., GA Technologies Report GA-A17056.

[11] M. Greenwald et al., in Proceedings of the 4th Int'l. Symp. on Heating in Toroidal Plasmas, Rome, Italy, 21-28 March 1984.

[12] H. F. Dylla et al., J. Nucl. Mater. 111 & 112 (1982) 211.

[13] H. F. Dylla et al., J. Nucl. Mater. 121 (1984) 144.

[14] D. Heifetz et al., J. Nucl. Mater. 121 (1984).

[15] F. Wagner et al., Phys. Rev. Lett. 49 (1982) 1408.

[16] M. G. Bell et al., J. Nucl. Mater. 121 (1984) 132.

[17] B. LeBlanc, B. Grek, and B. L. Stansfield, Bull. Am. Phys. Soc. 27 (1982) 1048.

[18] D. H. McNeill, M. G. Bell, B. Grek, and B. LeBlanc, Princeton Plasma Physics Laboratory Report PPPL-2085 (1984).

[19] S. L. Milora, G. L. Schmidt, et al., Nucl. Fusion 22 (1982) 1263.

[20] S. L. Milora, Oak Ridge National Laboratory Report ORNL/TM 8616 (1983).

[21] R. J. Hawryluk et al., Bull. Am. Phys. Soc. 27 (1982) 1046.

[22] D. K. Owens, R. J. Fonck, and D. S. Darrow, J. Nucl. Mater. 121 (1984) 344.

[23] B. L. Doyle, W. R. Wampler, H. F. Dylla, D. K. Owens, and M. L. Ulrickson, in Proceedings of 6th International Conference on Plasma Surface Interactions in Controlled Fusion Devices, to be published.

[24] D. K. Owens, S. M. Kaye, R. J. Fonck, and G. L. Schmidt, J. Nucl. Mater. 121 (1984) 29.

[25] R. Budny and D. Manos, J. Nucl. Mater. 121 (1984) 41.

Figure Captions

Fig.1 Neutral gas pressure as a function of line-averaged plasma density for closed divertor configuration with ohmic heating.

Fig.2 Plasma electron density and temperature profiles for an ohmically heated plasma before and after pellet injection.

Fig.3 Central chord visible continuum signals for pellet injection into discharges with different P_{INJ} and varying timing of the three pellets. The last pellet penetrates to r = 13,16,25, and 11 cm for cases a,b,c, and d, respectively.

Fig.4 Total energy deposited on outer neutralizer plate (NE) as a function of distance above the bottom of the neutralizer plate. The histogram reflects measurements from a thermocouple array on the neutralizer plate while the points indicate values derived from probe measurements of the divertor plasma.

Fig.5 Time evolution of line-averaged Z_{eff} from visible bremsstrahlung measurements for various configurations.

Fig.6 Visible bremsstranlung measurements of Z_{eff} after at least ~ 200 ms of neutral injection for several configurations.

Fig.7 Dilution-corrected impurity density estimates as a function of injected power.

Fig.8 Time evolution of Z_{eff} and the X-ray enhancement factor ζ during pellet injection as derived from X-ray PHA measurements. The decrease in impurity concentration appears to be stronger than that expected from dilution only.

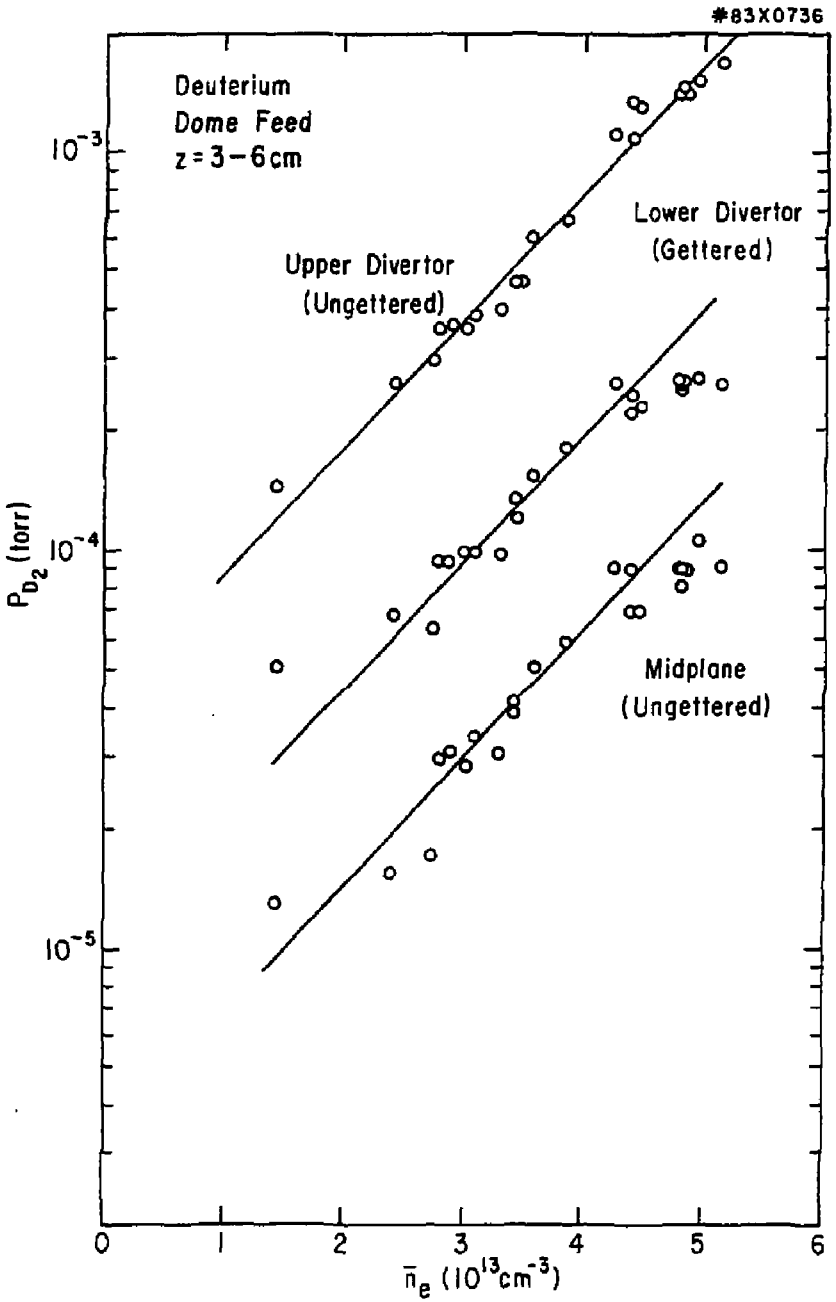
#83X0736
Deuterium
Dome Feed
z = 3 – 6cm
Upper Divertor
(Ungettered)
Lower Divertor
(Gettered)
Midplane
(Ungettered)
P_{D_2} (torr)
10^{-3}
10^{-4}
10^{-5}
0
1
2
3
4
5
6
$\bar{n}_e$ (10^{13}cm^{-3})

Figure 1

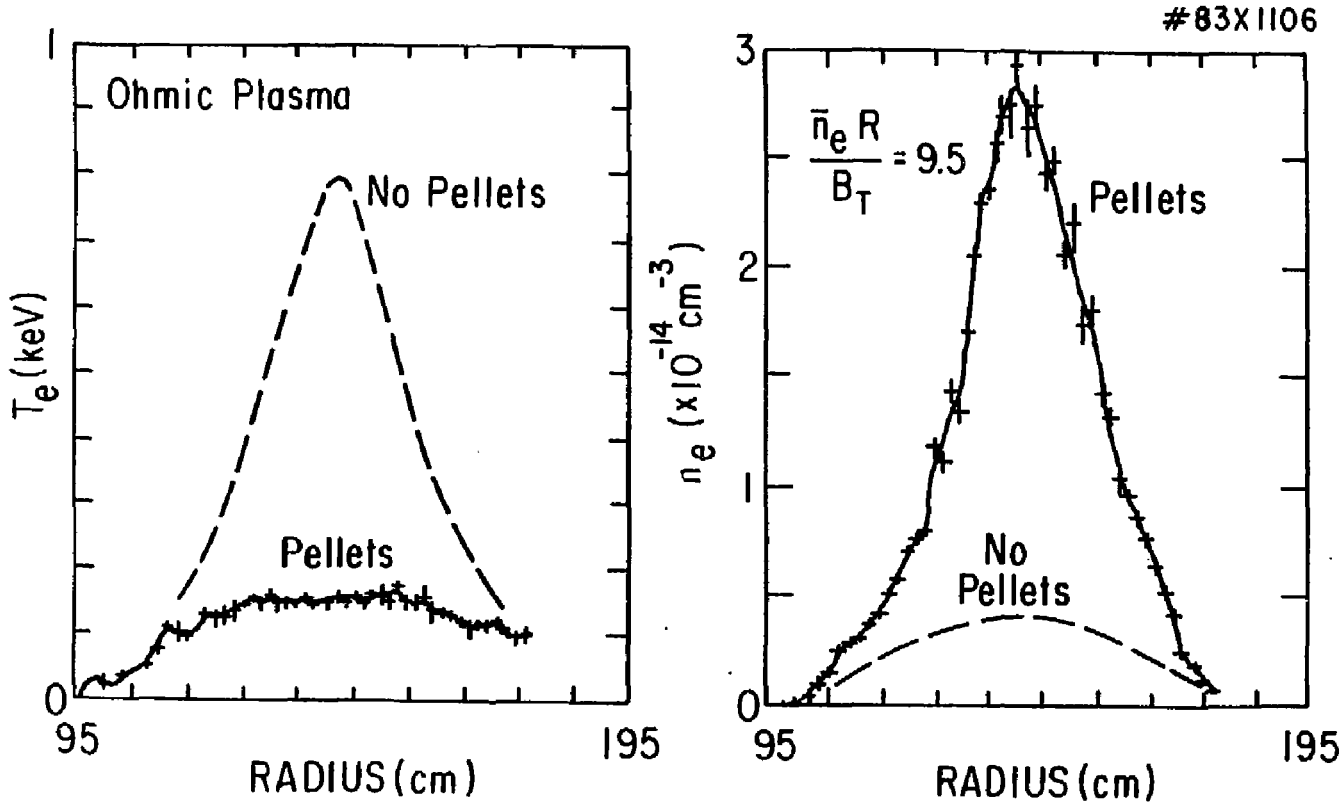
#83X1106
Ohmic Plasma
No Pellets
Pellets
T_e (keV)
1
0
95
195
RADIUS (cm)
$\frac{\bar{n}_e R}{B_T} = 9.5$
Pellets
No Pellets
n_e ($\times 10^{-14}$ cm^{-3})
3
2
1
0
95
195
RADIUS (cm)

Figure 2

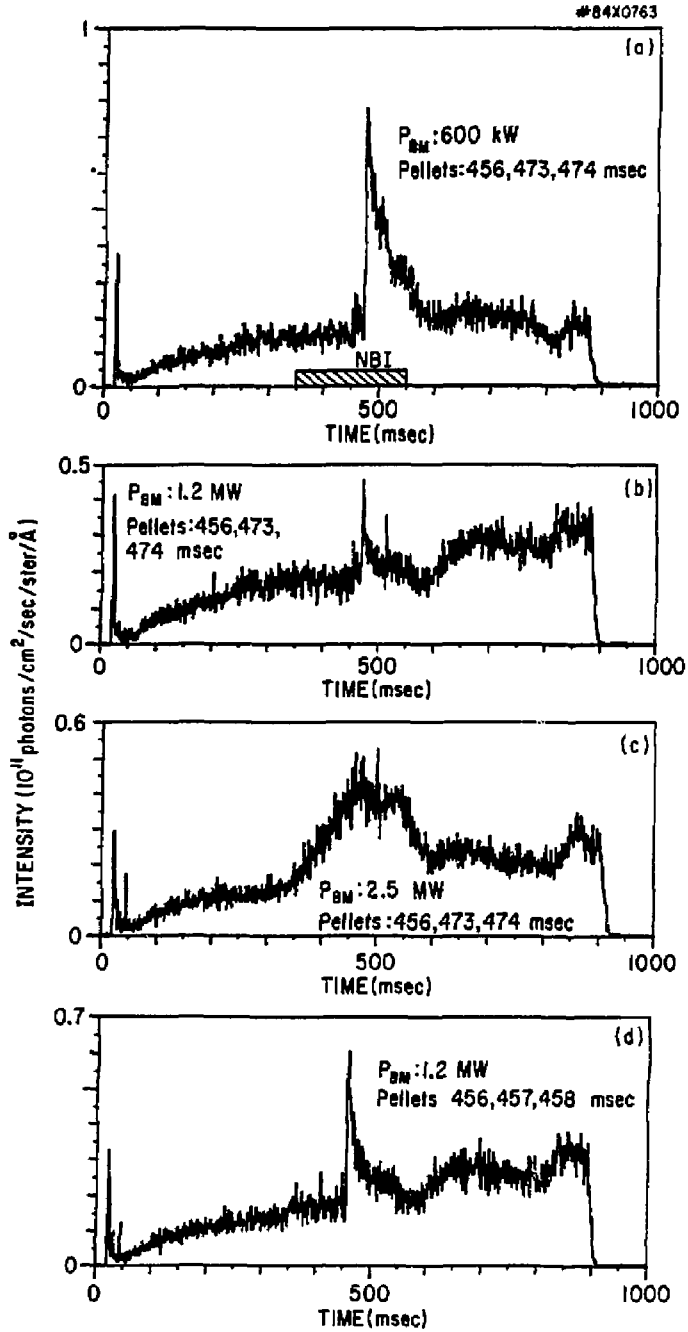
#84X0763
(a)
P_{BM}:600 kW
Pellets:456,473,474 msec
NBI
TIME(msec)
(b)
P_{BM}:1.2 MW
Pellets:456,473,
474 msec
(c)
P_{BM}:2.5 MW
Pellets:456,473,474 msec
(d)
P_{BM}:1.2 MW
Pellets 456,457,458 msec
INTENSITY (10^{11} photons/cm^2/sec/ster/Å)

Figure 3

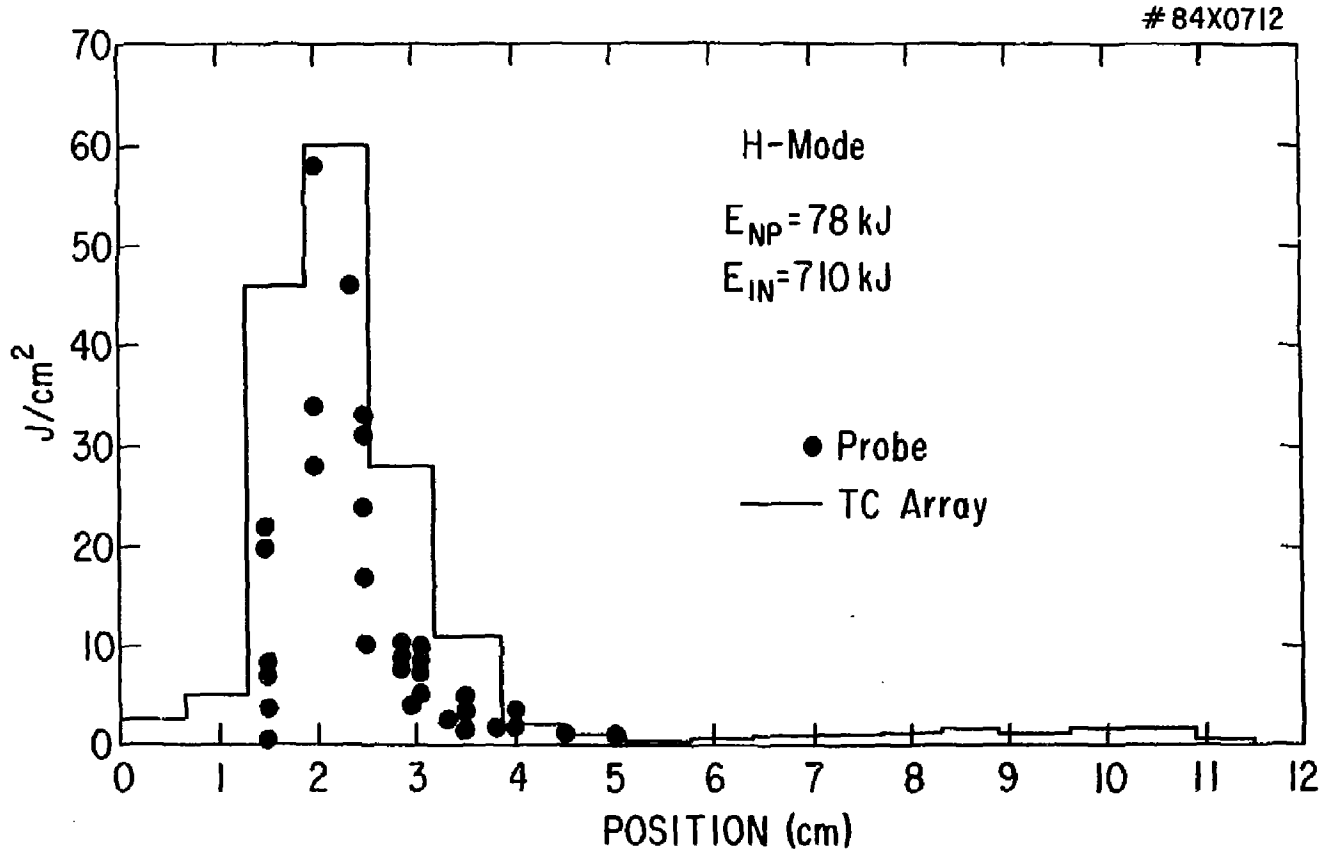
#84X0712
H-Mode
E_{NP}=78 kJ
E_{IN}=710 kJ
Probe
TC Array
J/cm^2
POSITION (cm)
0
10
20
30
40
50
60
70
0
1
2
3
4
5
6
7
8
9
10
11
12

Figure 4

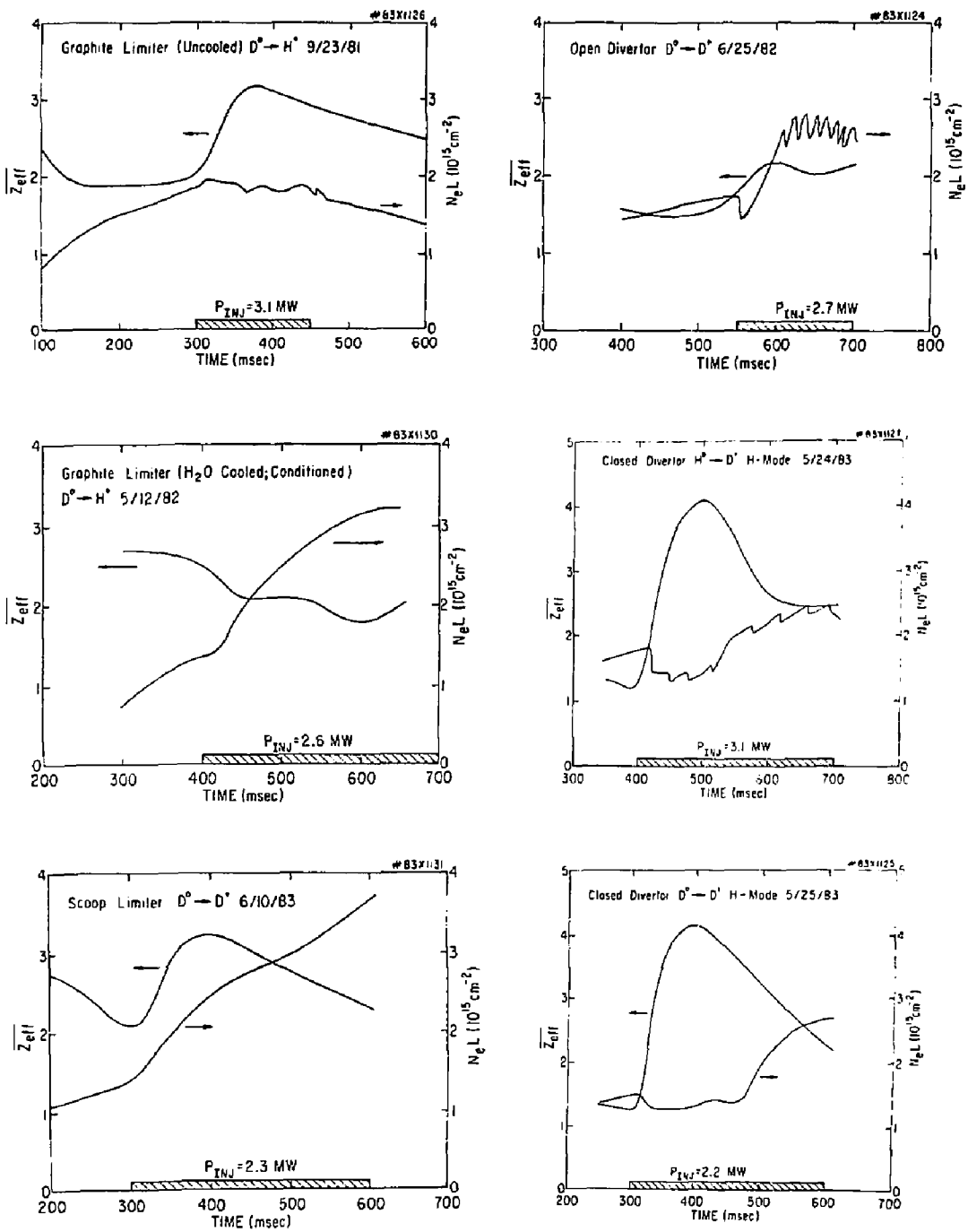
Graphite Limiter (Uncooled) D°→H° 9/23/81
P_{INJ}=3.1 MW
Open Divertor D°—D° 6/25/82
P_{INJ}=2.7 MW
Graphite Limiter (H_2O Cooled; Conditioned)
D°→H° 5/12/82
P_{INJ}=2.6 MW
Closed Divertor H°—D° H-Mode 5/24/83
P_{INJ}=3.1 MW
Scoop Limiter D°—D° 6/10/83
P_{INJ}=2.3 MW
Closed Divertor D°—D° H-Mode 5/25/83
P_{INJ}=2.2 MW
$\bar{Z}_{eff}$
N_eL ($10^{15}cm^{-2}$)
TIME (msec)

Figure 5

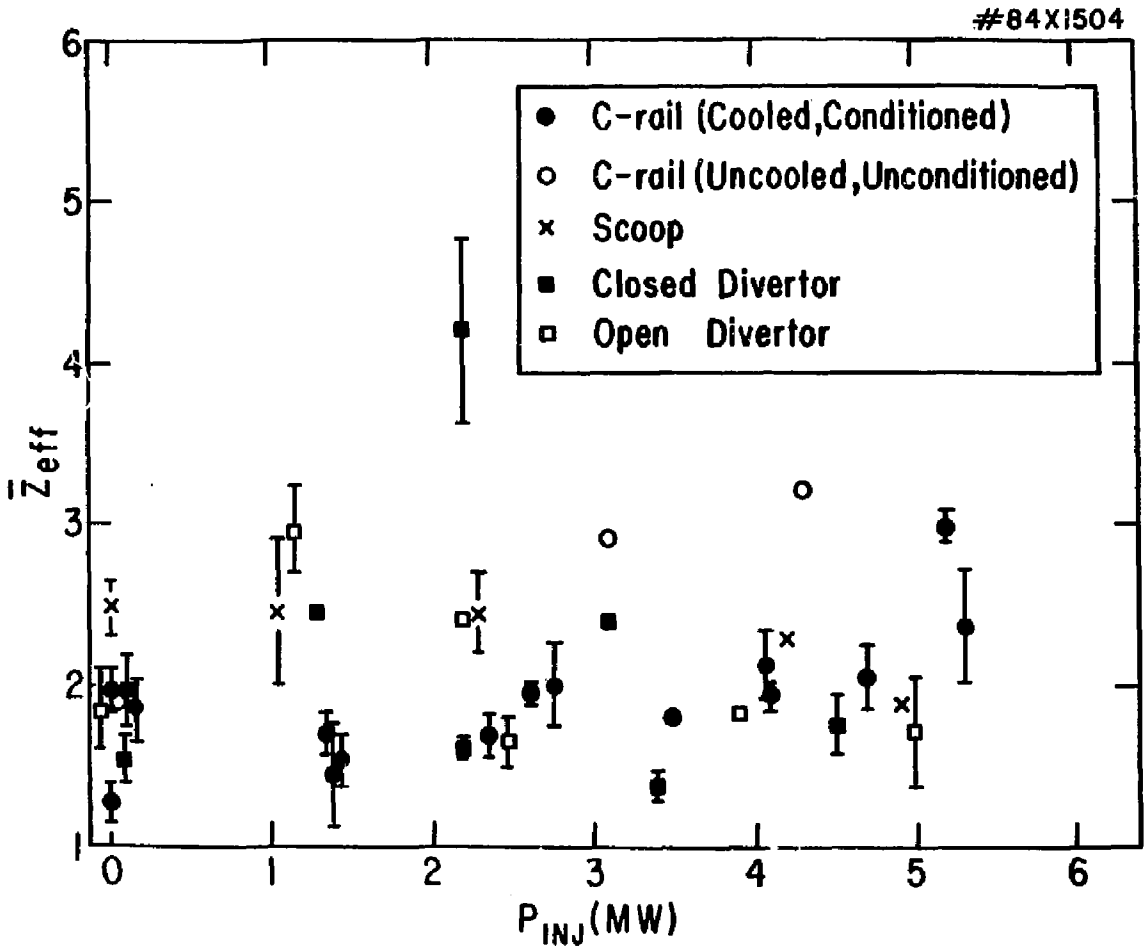
#84X1504
C-rail (Cooled,Conditioned)
C-rail (Uncooled,Unconditioned)
Scoop
Closed Divertor
Open Divertor
$\bar{Z}_{eff}$
P_{INJ}(MW)
1
2
3
4
5
6
0
1
2
3
4
5
6

Figure 6

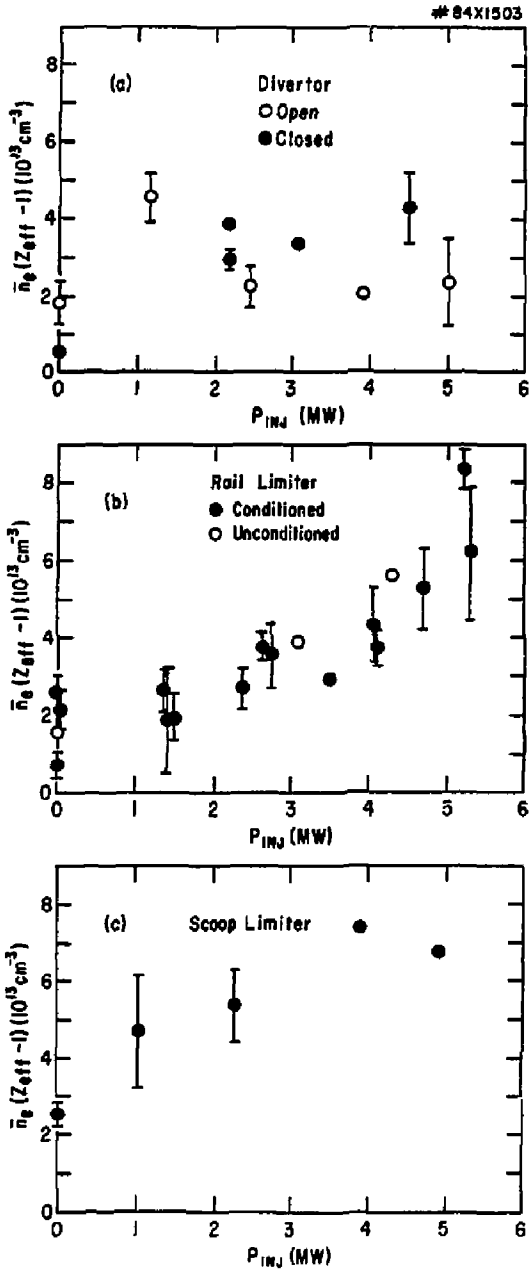
#84X1503
(a)
Divertor
Open
Closed
(b)
Rail Limiter
Conditioned
Unconditioned
(c)
Scoop Limiter
$\bar{n}_e (Z_{eff} - 1) (10^{13} cm^{-3})$
P_{INJ} (MW)

Figure 7

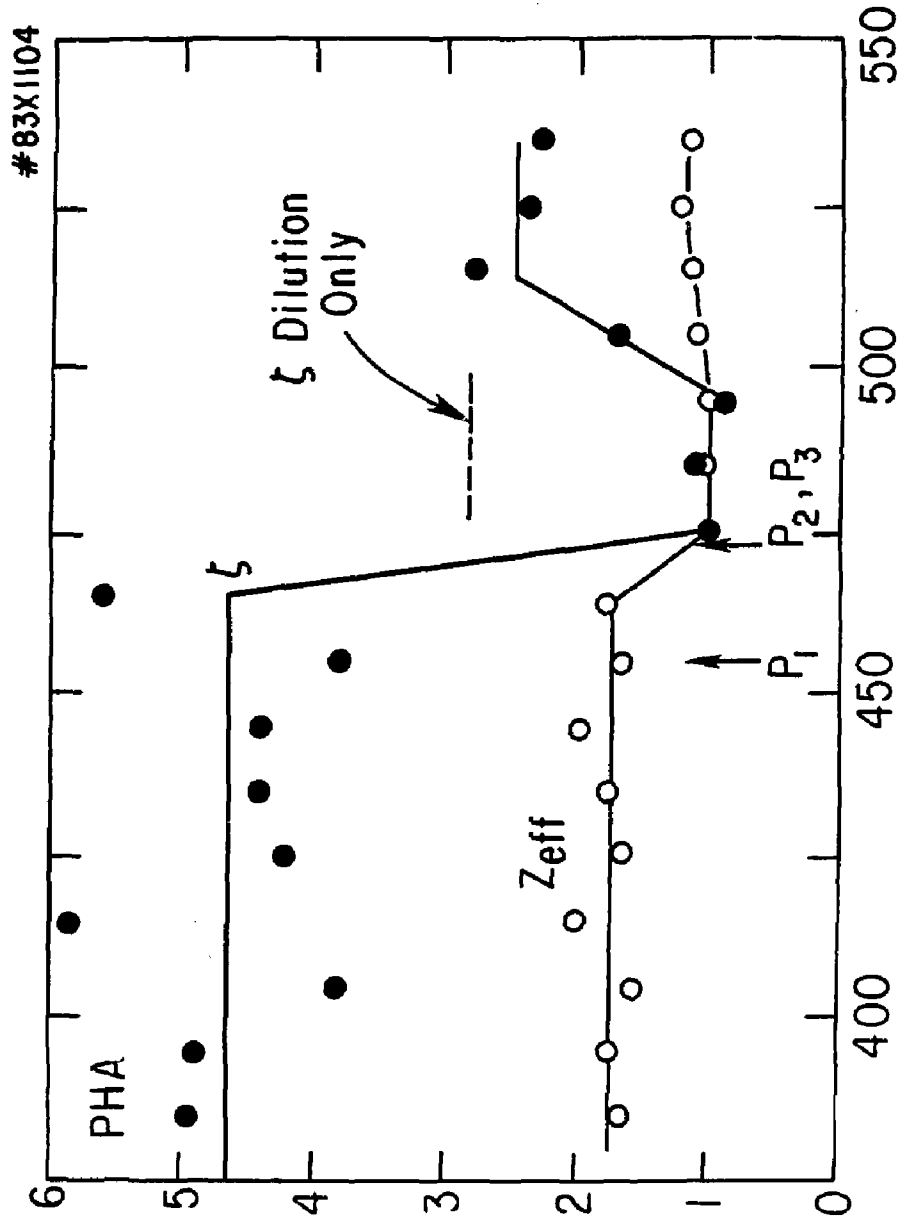
#83X1104
PHA
ζ
ζ Dilution Only
Z_{eff}
P_1
P_2, P_3
TIME (msec)
0
1
2
3
4
5
6
400
450
500
550

Figure 8

EXTERNAL DISTRIBUTION IN ADDITION TO TIC UC-20

Plasma Res Lab, Austra Nat'l Univ, AUSTRALIA
Dr. Frank J. Paoloni, Univ of Wollongong, AUSTRALIA
Prof. I.R. Jones, Flinders Univ., AUSTRALIA
Prof. M.H. Brennan, Univ Sydney, AUSTRALIA
Prof. F. Cap, Inst Theo Phys, AUSTRIA
Prof. Frank Verheest, Inst theoretische, BELGIUM
Dr. D. Palumbo, Dg XII fusion Prog, BELGIUM
Ecole Royale Militaire, Lab de Phys Plasmas, BELGIUM
Dr. P.H. Sakanaka, Univ Estadual, BRAZIL
Dr. C.R. James, Univ of Alberta, CANADA
Prof. J. Teichmann, Univ of Montreal, CANADA
Dr. H.M. Skarsgard, Univ of Saskatchewan, CANADA
Prof. S.R. Sreenivasan, University of Calgary, CANADA
Prof. Tudor W. Johnston, INRS-Energie, CANADA
Dr. Hannes Barnard, Univ British Columbia, CANADA
Dr. M.P. Bachynski, MPB Technologies, Inc., CANADA
Zhengwu Li, SW Inst Physics, CHINA
Library, Tsing Hua University, CHINA
Librarian, Institute of Physics, CHINA
Inst Plasma Phys, Academia Sinica, CHINA
Dr. Peter Lukac, Komenskeho Univ, CZECHOSLOVAKIA
The Librarian, Culham Laboratory, ENGLAND
Prof. Schatzman, Observatoire de Nice, FRANCE
J. Radet, CEN-BP6, FRANCE
AM Dupas Library, AM Dupas Library, FRANCE
Dr. Tom Mual, Academy Bibliographic, HONG KONG
Preprint Library, Cent Res Inst Phys, HUNGARY
Dr. S.K. Trehan, Panjab University, INDIA
Dr. Indra, Mohan Lal Das, Banaras Hindu Univ, INDIA
Dr. L.K. Chavda, South Gujarat Univ, INDIA
Dr. R.K. Chhajlani, Var Ruchi Marg, INDIA
P. Kaw, Physical Research Lab, INDIA
Dr. Phillip Rosenau, Israel Inst Tech, ISRAEL
Prof. S. Cuperman, Tel Aviv University, ISRAEL
Prof. G. Rostagni, Univ Di Padova, ITALY
Librarian, Int'l Ctr Theo Phys, ITALY
Miss Clelia De Palo, Assoc EURATOM-CNEN, ITALY
Biblioteca, del CNR EURATOM, ITALY
Dr. H. Yamato, Toshiba Res & Dev, JAPAN
Prof. M. Yoshikawa, JAERI, Tokai Res Est, JAPAN
Prof. T. Uchida, University of Tokyo, JAPAN
Research Info Center, Nagoya University, JAPAN
Prof. Kyoji Nishikawa, Univ of Hiroshima, JAPAN
Prof. Sigeru Mori, JAERI, JAPAN
Library, Kyoto University, JAPAN
Prof. Ichiro Kawakami, Nihon Univ, JAPAN
Prof. Satoshi Itoh, Kyushu University, JAPAN
Tech Info Division, Korea Atomic Energy, KOREA
Dr. R. England, Ciydad Universitaria, MEXICO
Bibliotheek, Fom-Inst Voor Plasma, NETHERLANDS
Prof. B.S. Liley, University of Waikato, NEW ZEALAND
Dr. Suresh C. Sharma, Univ of Calabar, NIGERIA
Prof. J.A.C. Cabral, Inst Superior Tech, PORTUGAL
Dr. Octavian Petrus, ALI CUZA University, ROMANIA
Prof. M.A. Hellberg, University of Natal, SO AFRICA
Dr. Johan de Villiers, Atomic Energy Bd, SO AFRICA
Fusion Div, Library, JEN, SPAIN
Prof. Hans Wilhelmson, Chalmers Univ Tech, SWEDEN
Dr. Lennart Stenflo, University of UMEA, SWEDEN
Library, Royal Inst Tech, SWEDEN
Dr. Erik T. Karlson, Uppsala Universitet, SWEDEN
Centre de Recherchesen, Ecole Polytech Fed, SWITZERLAND
Dr. W.L. Weise, Nat'l Bur Stand, USA
Dr. W.M. Stacey, Georg Inst Tech, USA
Dr. S.T. Wu, Univ Alabama, USA
Prof. Norman L. Oleson, Univ S Florida, USA
Dr. Benjamin Ma, Iowa State Univ, USA
Prof. Magne Kristiansen, Texas Tech Univ, USA
Dr. Raymond Askew, Auburn Univ, USA
Dr. V.T. Tolok, Kharkov Phys Tech Ins, USSR
Dr. D.D. Ryutov, Siberian Acad Sci, USSR
Dr. G.A. Eliseev, Kurchatov Institute, USSR
Dr. V.A. Glukhikh, Inst Electro-Physical, USSR
Institute Gen. Physics, USSR
Prof. T.J. Boyd, Univ College N Wales, WALES
Dr. K. Schindler, Ruhr Universitat, W. GERMANY
Nuclear Res Estab, Julich Ltd, W. GERMANY
Librarian, Max-Planck Institut, W. GERMANY
Dr. H.J. Kaeppler, University Stuttgart, W. GERMANY
Bibliothek, Inst Plasmaforschung, W. GERMANY